ARTICLE OPEN

Check for updates

A myeloid-dormant metabolic transcriptome identifies a poor-prognosis subgroup in hyperdiploid multiple myeloma with targetable vulnerabilities

Naroa Barrena[1,8], Edurne San José-Enériz[2,3,4,8], Luis V. Valcárcel[1,2], Danel Olaverri-Mendizabal[1], Estibaliz Urizar-Compains[2,3], Leire Garate[3,4,5], Estíbaliz Miranda[2,3,4], Paula Rodriguez-Marquez[2,4], Romika Kumari[6], Patxi San Martín-Uriz[2,3], Juan Roberto Rodriguez-Madoz[2,4], Leonor Puchades-Carrasco[7], Caroline A. Heckman[6], Paula Rodriguez-Otero[3,4,5], Francisco J. Planes[1,9]✉, Xabier Agirre[2,3,4,9]✉ and Felipe Prósper[2,3,4,5,9]✉

© The Author(s) 2026

Aberrant metabolism, a hallmark of cancer, reveals vulnerabilities across human tumors. Here, we demonstrate that transcriptomic alterations of metabolism-related genes (metabolic transcriptome) in multiple myeloma (MM), classify patients into six metabolic-transcriptional groups characterized by specific metabolic pathways and cytogenetic alterations, independent of currently described myeloma risk groups. Interestingly, hyperdiploid patients clustered into 2 groups (MM5 and MM6) with significantly distinct Progression-Free and Overall Survival. The MM5 group, with worse prognosis, showed a significant enrichment in myeloid and dormant cell signatures. Regulon analysis identified myeloid transcription factors (TFs) as regulators of metabolic, myeloid, and dormant genes in MM5. In addition to myeloid genes acting as potential biomarkers and therapeutic targets, the metabolic gene *ACSL1* plays a crucial role in MM5, decreasing cell proliferation by affecting metabolism and mitochondrial function, sensitizing MM to BCL-2 family inhibitors. These findings highlight ACSL1 as a promising therapeutic target for MM5 and provide new insights into MM metabolic heterogeneity that may guide future precision medicine strategies.

Blood Cancer Journal (2026)16:169 ; https://doi.org/10.1038/s41408-026-01604-w

INTRODUCTION

Multiple myeloma (MM) is a hematologic neoplasm characterized by the uncontrolled proliferation of clonal plasma cells (PCs) within the bone marrow. Despite significant advances in treatment over the past years, which have notably improved patient survival, MM remains, for the most part, an incurable disease [1]. This is in part due to the heterogeneity of the disease characterized by numerous gene translocations and mutations that lead to tumor development and progression, ultimately contributing to drug resistance [2]. Based on these genetic alterations, MM patients can be classified into two main subgroups: hyperdiploid MM (H-MM) and non-hyperdiploid MM (NH-MM). H-MM is characterized by the presence of multiple trisomies of odd-numbered chromosomes, whereas NH-MM is defined by chromosome translocations. In NH-MM, these translocations juxtapose IgH enhancers with various oncogenes, such as *CCND1* in t(11;14), occurring in approximately 20% of patients, or *FGFR3/MMSET* in t(4;14), observed in about 10% of cases. Less frequently, translocations involve *MAF* in t(14;16), *MAFB* in t(14;20), and *CCND3* in t(6;14) [3]. Due to this genetic heterogeneity among tumor PCs, it is necessary to investigate their biology through alternative and complementary perspectives in order to identify novel biomarkers that could enhance the stratification of MM patients and could facilitate the development of new targeted therapeutic strategies designed to improve both treatment efficacy and the overall quality of life for patients with MM.

In addition to genetic abnormalities, metabolic reprogramming represents a critical hallmark of cancer cells, which enables them to acquire and sustain malignant characteristics, thereby supporting their aggressiveness and persistence [4]. While metabolic changes have been well-documented in various solid tumors such as lung cancer [5], breast [6], or prostate [7], studies on metabolic alterations in hematological malignancies, including MM, are less frequent. Though emerging evidence supports their role in MM pathogenesis [8, 9], the availability of large-scale metabolomic studies in MM is currently limited. Large-scale transcriptomic datasets in MM provide an alternative approach to investigate metabolism-associated genes through the analysis of their expression profiles.

In this study, we have analyzed the transcriptome of metabolism-related genes (metabolic transcriptome) in MM

[1]TECNUN, Universidad de Navarra, San Sebastián, Spain. [2]Hemato-Oncology Program, CIMA Universidad de Navarra, IDISNA, Pamplona, Spain. [3]Cancer Centre Clínica Universidad de Navarra (CCUN), Pamplona, Navarra, España. [4]Centro de Investigación Biomédica en Red Cáncer (CIBERONC), Madrid, Spain. [5]Departmento de Hematología y Terapia Celular, Clínica Universidad de Navarra, Universidad de Navarra, IdISNA, Pamplona, Spain. [6]Institute for Molecular Medicine Finland - FIMM, HiLIFE - Helsinki Institute of Life Science, iCAN Digital Cancer Medicine Flagship, University of Helsinki, Helsinki, Finland. [7]Drug Discovery Unit, Instituto de Investigación Sanitaria La Fe, Valencia, Spain. [8]These authors contributed equally: Naroa Barrena, Edurne San José-Enériz. [9]These authors contributed equally: Francisco J. Planes, Xabier Agirre, Felipe Prósper. ✉email: fplanes@unav.es; xaguirre@unav.es; fprosper@unav.es

Received: 3 November 2025 Revised: 23 July 2026 Accepted: 31 July 2026
Published online: 11 August 2026

patients, revealing significant heterogeneity in the expression of metabolism-associated genes, which closely correlates with common cytogenetic alterations. The identified metabolic transcriptomic signatures allowed MM patient stratification, indicating potential new metabolic biomarkers and therapeutic targets for the treatment of MM patients.

MATERIALS AND METHODS

Gene expression

Gene expression data were obtained from: i) RNA-seq data from multiple sources, including the MMRF-CoMMpass cohort, the different B cell subpopulations samples [10], the small cohort of MM samples [11], and the cohort from the study of the University of Helsinki [8], and ii) microarray data from the HOVON-65/GMMG-HD4 cohort [12]. The RNA-seq data of different B cell subpopulations (GSE114816) [10] and MM samples (GSE151063) [11] were obtained from GEO. In addition, gene expression data from the Institute for Molecular Medicine Finland (FIMM) cohort were directly provided by the authors [8]. Microarray data from the HOVON-65/GMMG-HD4 cohort is publicly available in GEO (GSE19784) [12]. We recalculated gene expression data from the raw CEL files using the aroma.affymetrix R framework [13], applying RMA normalization. For gene-level summarization across probe sets, we employed a custom CDF (Chip Definition File) for the Affymetrix Human Genome U133 Plus 2.0 Array, provided by the MicroArray Lab (http://brainarray.mbni.med.umich.edu/Brainarray/).

NMF clustering analysis and signature generation

Clustering analysis was performed using the CoMMpass dataset. The subset of 2753 genes obtained from Possemato et al. [14], was filtered according to the following criteria: i) genes with a 95th percentile of expression greater than 2 TPM are retained; and ii) genes with bimodal index of the expression greater than 1.1 were included [15]. The Non-Negative Matrix Factorization (NMF) algorithm [16] was applied to the resulting subset of genes using the *NMF* R package with default parameters. See Supplementary material and methods.

Gene Set Enrichment Analysis (GSEA)

We performed differential gene expression analysis across the transcriptome of all coding genes using the same approach as employed for the signature generation (*limma-voom* pipeline). The resulting *t*-statistics were used to rank all genes for each cluster. Gene-to-pathway associations were derived from KEGG and Reactome subsets of canonical pathways available in the Molecular Signatures Database (MSigDB) [17, 18]. Gene Set Enrichment Analysis (GSEA) was conducted using the ranked gene lists for each cluster and the KEGG and Reactome gene sets, implemented via the *fgsea* R package. Finally, we selected the top 5 most differentially enriched pathways with a positive Normalized Enrichment Score (NES) for each group.

Survival analysis

All survival analyses were visualized using Kaplan-Meier curves, generated with the *survival* and *survminer* R packages. A summary of the main treatment regimens administered to patients from the CoMMpass cohort is provided in Supplementary Table 1. See Supplementary material and methods.

Gene Set Variation Analysis

Gene Set Variation Analysis (GSVA) [19] was performed using the hematopoietic progenitor cell marker gene sets obtained from Ainciburu. M. et al. [20] and Wu, J. et al. [21], and the *GSVA* R package was used to compute and visualize gene set enrichment scores at the single-sample level.

TraRe regulon analysis

TraRe (Transcriptional Rewiring) algorithm [22] was employed to identify module-based gene regulatory network (GRN) deregulation between the groups MM5 and MM6, as well as to detect specific rewired regulons. Specifically, the function *LINKER_run* was applied to log2-normalized counts of MM5 and MM6 patients using a list of TF regulators [23], with the parameter $Nr_bootstraps = 50$. Then, we ran the function *rewiring_regulon_level*, obtaining a list of regulons with their drivers and target genes. From this output, we searched for drivers that were myeloid TFs and their associated list of targets.

Hyperdiploid biomarker definition

From the CoMMpass cohort, we first selected all the patients that belong to MM5 or MM6 groups and separated them randomly in 80% training set and a 20% test set, maintaining the proportions. See Supplementary material and methods.

CD13 inhibition

JJN-3 cells were treated with 5 µM or 10 µM of Bestatin (HY-B0134A, MedChemExpress), a CD13 inhibitor, for 48 hours. Cells were washed twice, resuspended in PBS (1×10^6cells/mL), and incubated with 20 µl of PE CD13 antibody (347406, BD Pharmingen) for 30 min at room temperature in the dark. After washing, cells were collected on a BD FACSCanto II flow cytometer (Becton Dickinson, San Jose, CA, USA) and analyzed using FlowJo software.

CAR T cell generation and cytotoxicity assay

Second-generation BCMA and CD33 CAR constructs were used [24, 25]. CAR structure comprised the scFv or single-domain antibody-based (sdAb) targeting BCMA or CD33, respectively, CD8 hinge and TMD, 4-1BB and CD3ζ domains fused to a BFP reporter gene. Lentiviral vectors were produced in HEK293T cells, and CAR-T cells were generated from healthy donors as described [24]. See Supplementary material and methods.

CRISPR-Cas9 ACSL1 knockout

Stable Cas9-expressing KMS-28-BM and MM.1S cell lines were generated via lentiviral transduction with the Lenti-Cas9-2A-Blast vector (Addgene, #73310) and selected with 17.5 µg/ml blasticidin (Invitrogen) for 7 days. For *ACSL1* knockout, sgRNAs (sgACSL1-1: 5′-GTTTCCGAGAGCCTAAACAA-3′; sgACSL1-2: 5′-CAAGAGCCATCGCTTCAGCG-3′) were cloned into the CRISPseq-BFP vector (Addgene, #85707). Lentiviruses were produced in HEK293T cells by co-transfection with sgRNA plasmids, pMD2G (Addgene, #12259) and psPAX2 (Addgene, #12260) using Lipofectamine 2000 (Invitrogen). Constitutively Cas9-expressing cell lines were infected at MOI 1 with 4 µg/µl Polybrene (Sigma). BFP+ cells and viable cells were determined by flow cytometry using the BD FACSCanto II (BD Biosciences) 72 hours after infection. Then, every two days, the number of BFP+ living cells was determined by FACS. As a control, we used cells infected with the empty CRISPseq-BFP-backbone (scramble, Scr).

Western blot

To evaluate the efficiency of the ACSL1 knockout experiments, we assessed ACSL1 protein levels via Western blot 7 days after lentiviral infection. Protein extraction, quantification, and Western blot were performed as previously described [26]. See Supplementary material and methods.

RNA-seq sequencing

Transcriptomic analyses were performed in MM.1S and KMS-28-BM cells after ACSL1 knockout using two specific CRISPR-Cas9 guides. BFP+ cells were previously sorted at day 6 (MM.1S) or day 10 (KMS-28-BM) post-infection. Batch effects across samples were corrected using Combat-seq [27]. The differential gene expression analysis was performed with the edgeR algorithm. See Supplementary material and methods.

Oxygen consumption rate (OCR) and Extracellular acidification rate (ECAR)

OCR and ECAR were measured in an XFp Extracellular flux analyzer (Seahorse Biosciences) after ACSL1 knockdown via CRISPR-Cas9 in MM.1S (day 6 post-infection) and KMS-28-BM (day 10 post-infection). See Supplementary material and methods.

Combination assays

To evaluate the effect of ACSL1 inhibition by CRISPR-Cas9 combined with Venetoclax or S63845 (MedChemExpress), MM.1S and KMS-28-BM cells were first infected with two different guides targeting ACSL1. Six (MM.1S) or 10 days (KMS-28-BM) post-infection, cells were treated with the compounds (15 µM Venetoclax or 500 nM S63845 for MM.1S and 300 nM

Venetoclax or 1000 nM S63845 for KMS-28-BM). See Supplementary material and methods.

Xenograft in vivo experiments

In vivo xenograft experiments evaluating the functional role of ACSL1 and its therapeutic targeting in combination with Venetoclax or S63845 are described in the Supplementary material and methods.

Statistical analysis

Normality was assessed using the Shapiro–Wilk test. Comparisons were made with the Mann–Whitney U-test (for unpaired samples without a normal distribution) and Student's t-test (for paired samples showing a Gaussian distribution). In the case of combination assays between ACSL1 inhibition by CRISPR-Cas9 and Venetoclax/S63845 inhibitors, p-values were determined by one-way analysis of variance (ANOVA), followed by Tukey's multiple comparison test. GraphPad Prism 6.0 was used. *P*-value < 0.05 was considered to be indicative of statistically significant differences.

RESULTS

Metabolic classification of MM

To explore the role of metabolic reprogramming in MM, we analyze the expression of 2753 metabolic genes [14] involved in human cellular metabolism (metabolic transcriptome) in PC from MM patients (MM-PC) as well as different B-cell populations [10, 26] (Supplementary Fig. 1A). Principal component analysis (PCA) revealed that the metabolic transcriptome of PCs (including tonsillar and bone marrow PCs from healthy donors and MM-PCs) was markedly different from B cell subpopulations (including naive B cells, centroblasts, centrocytes and memory B cells) (Fig. 1A). We also observed that although MM-PCs maintain a similar metabolic profile as healthy BM-PC, MM-PCs further exhibited a large inter-patient metabolic transcriptional heterogeneity (Fig. 1A). To study this heterogeneity, we analyzed the expression of the 2,753 genes using RNA-seq data from 619 patients of MMRF-CoMMpass cohort (Fig. 1B). We filtered metabolic genes based on their expression level (quantile 95% ≥ 2 TPM) and bimodal index (≥1.1), resulting in 186 metabolic genes. We then performed Non-Negative Matrix Factorization clustering (NMF) [16] and based on the cophenetic correlation coefficient results (see Methods section), MM patients were classified into six unique transcriptional metabolic groups (Fig. 1B). Then, using the expression of those 186 genes, we conducted a differential expression analysis, comparing each cluster against the mean of the remaining clusters (logFC ≥ 1 and an *adjusted p.value* ≤ 0.01), to define the upregulated metabolic transcriptomic signature of each MM group. This analysis identified 30 over-expressed metabolic genes in cluster MM1, 26 in cluster MM2, 21 in cluster MM3, 22 in cluster MM4, 40 in cluster MM5, and 26 genes in cluster MM6 (Fig. 1C**;** Supplementary Table 2). Gene Set Enrichment Analysis (GSEA) revealed that each group was characterized by abnormalities in distinct metabolic pathways: MM1 group was associated with altered inositol phosphate metabolism, MM2 group with glycan metabolism, MM3 group with cholesterol biosynthesis, MM4 group was enriched in gluconeogenesis, MM5 group exhibited positive enrichment in arachidonic acid and fatty acid metabolism and finally, MM6 showed an enrichment in amino acid metabolism (Fig. 1D**;** Supplementary Table 3). These results indicate that MM patients can be classified in defined transcriptional metabolic groups.

MM transcriptional metabolic groups were significantly associated ($p < 0.05$) with well-defined cytogenetic alterations in MM (Supplementary Table 4): MM1 was associated with MM patients harboring t(11;14), t(12;14) or t(6;14), involving genes from the cyclin D family (*CCND1*, *CCND2*, *CCND3*); MM2 group correlated with MM patients with t(4;14); MM3 group was linked to t(14;16), t(14;20) or t(8;14), which encompass genes of the family of transcription factors *MAF* (*MAF*, *MAFA*, *MAFB*); MM4 was associated with hyperdiploidy, amp(1q) and t(8;14), involving the *MYC* gene; and finally, the MM5 and MM6 groups primarily included MM patients with the most relevant characteristic being uniquely the hyperdiploidy (Fig. 1E). No correlation was observed between metabolic groups and the most common gene mutations identified in MM (Supplementary Fig. 1B) or with the standard risk classifications (R-ISS) or the recently described definition of high risk myeloma [28, 29] (Supplementary Fig. 1C-D). Furthermore, the six MM transcriptional metabolic groups were validated in two independent MM patient cohorts (Supplementary Fig. 1A, E, F). In summary, these results demonstrate that MM patients exhibit a heterogeneous metabolic transcriptome, which classifies them into six distinct groups with unique metabolic characteristics and specific cytogenetic alterations.

PC from patients in group MM5 are characterized by the expression of a myeloid and dormant cell signature

Although the six identified metabolic groups exhibited distinct metabolic transcriptome profiles, an intriguing observation was that MM5 and MM6 groups, despite sharing the same cytogenetic characteristic of hyperdiploidy, displayed markedly different metabolic transcriptomes (Fig. 1C–E). Furthermore, these two metabolic groups showed significantly different Progression Free Survival (PFS) (*p-value* = 0.023) and Overall Survival (OS) (*p-value* = 0.007), with a significantly worse prognosis for patients in group MM5 (Fig. 2A).

In order to understand these differences, we compared the transcriptome of MM patients from groups MM5 and MM6. GSEA revealed that group MM5 was characterized by a significant enrichment in pathways related to myeloid cell categories (Fig. 2B, Supplementary Table 5). Differential expression analysis identified 2,385 significantly upregulated and 359 downregulated genes in the MM5 group compared to the MM6 group. Among significantly upregulated genes, we detected distinct myeloid cell markers and a significant enrichment in Gene Ontology (GO) terms related to myeloid cells (Fig. 2C, D). We also performed a GSVA using the expression of hematopoietic cell markers identified using scRNA-seq by Ainciburu et al [20]. This analysis revealed a clear enrichment of gene markers related to distinct and specific myeloid progenitors and myeloid cells and significant upregulation of genes specific to myeloid cells (erythroid, monocyte, and neutrophil) in PC from group MM5 (Fig. 2E).

To further investigate whether the myeloid-like signature identified in MM5 reflected intrinsic features of tumor PCs rather than contamination by non-PC populations, we analyzed independent single-cell RNA-sequencing datasets from MM patients across four cohorts [30–33] (Supplementary Fig. 2A). Cell annotation identified distinct hematopoietic populations, including PCs, B cells, NK cells, T cells, progenitors and myeloid cells (Supplementary Fig. 2B). PCs expressing canonical markers such as *MZB1* and *SDC1* also exhibited heterogeneous expression of genes typically associated with myeloid or non-PC lineages, including *HBB*, *HBD*, *LYZ*, *S100A4* and *CD33* (Supplementary Fig. 2C). These expression patterns were consistently observed across independent cohorts, supporting that the myeloid-like transcriptional program identified in MM5 reflects an intrinsic feature of a subset of MM PCs rather than a contamination artifact.

A possible explanation for this myeloid-related signature could be the presence of dormant cells, as MM dormant cells have been described to express a transcriptome signature enriched in immune-related genes and genes associated with myeloid cell differentiation [34]. Indeed, PC from group MM5 showed an upregulation of specific markers of dormant cells with a significant enrichment in dormant transcriptome signature in comparison with group MM6 (Fig. 2F). In summary, PCs from the MM5 hyperdiploid group, in addition to their specific metabolic transcriptome, exhibited characteristics of both myeloid progenitor and dormant cells, which might explain the adverse prognosis of these patients.

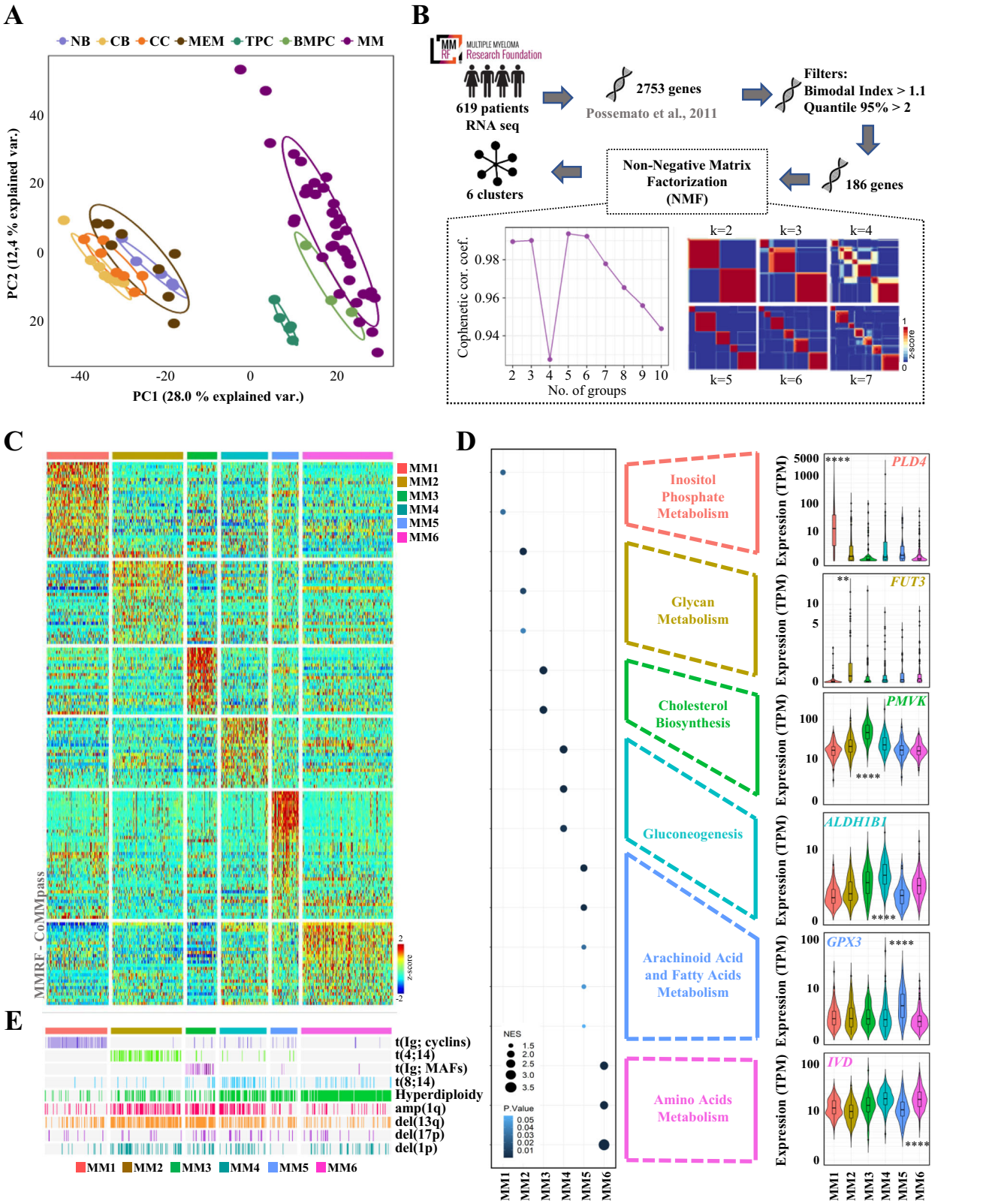

Fig. 1 Metabolic transcriptome of MM is altered and reveals six different metabolic subtypes. A Principal Component Analysis (PCA) with the 2,753 metabolism-related genes in the cohort of B cell subpopulations (NB: Naïve B cells; CB: Centroblast B cells; CC: Centrocyte B cells; MEM: Memory B cells; TPC: Tonsillar plasma cells; BMPC: Bone marrow plasma cells) and MM samples. Genes with no expression or variance across the cohort were filtered out. **B** Pipeline used in this study for unsupervised clustering and identification of novel metabolic groups. **C** Heatmap of the six metabolic clusters identified in 619 MM patients from the CoMMpass cohort using NMF. Each column annotation represents a distinct metabolic cluster, while rows correspond to metabolic gene signatures. Gene expression is scaled across patients. **D** GSEA results highlighting significantly enriched pathways in each cluster, along with boxplots showing TPM expression levels of key genes in each pathway. **E** Cytogenetic alterations in 619 MM patients of the CoMMpass cohort.

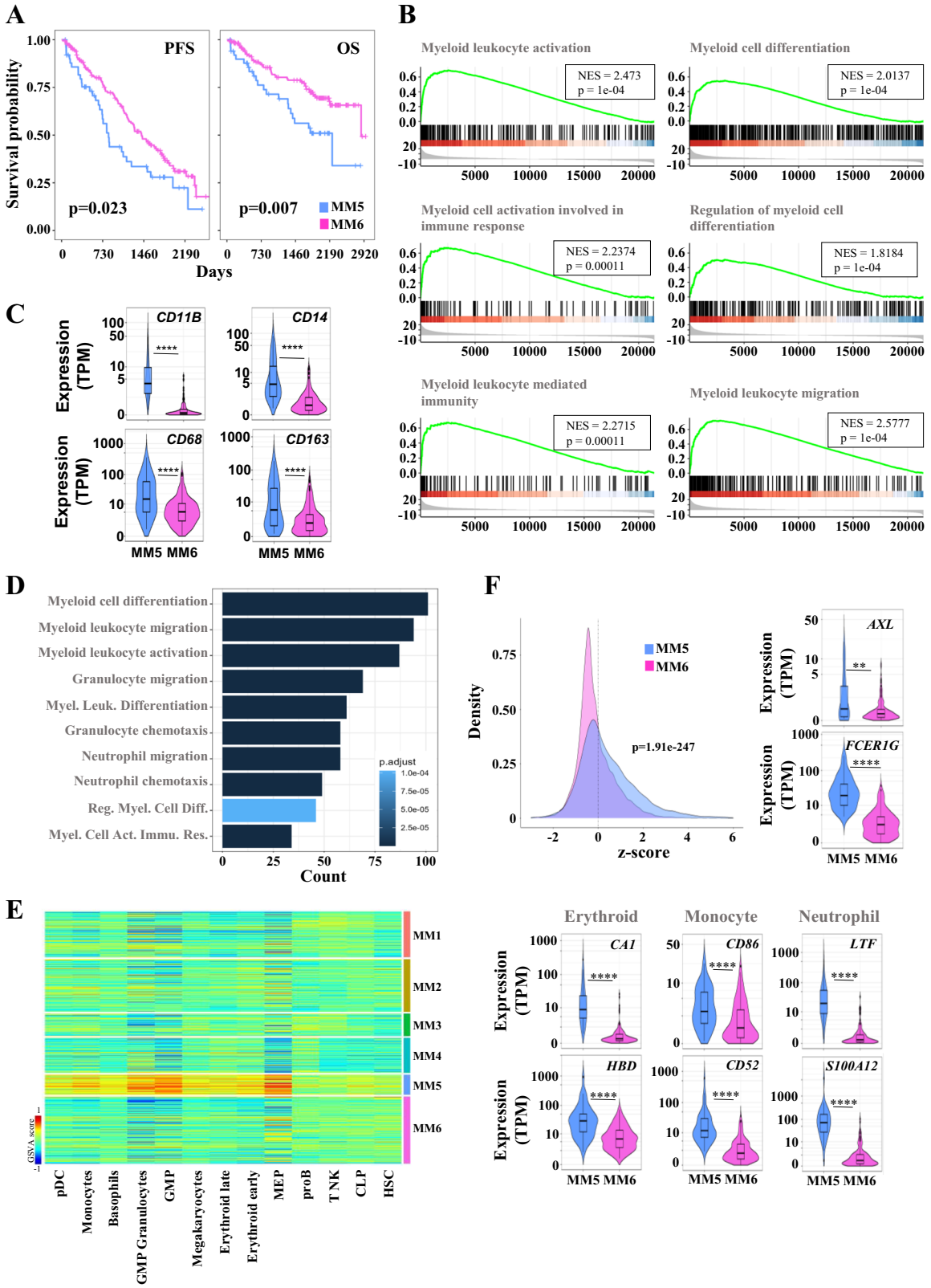

Fig. 2 Study of the prognosis of the six metabolic groups of MM and differences among hyperdiploid groups. A Progression Free Survival (PFS) and Overall survival (OS) analysis of MM patients from the CoMMpass cohort belonging to the MM5 and MM6 groups. **B** GSEA enrichment plots of the gene sets related to myeloid categories. **C** Boxplots showing the expression of myeloid markers in MM5 and MM6 groups. **D** Gene Ontology (GO) enrichment analysis of overexpressed genes in MM5 compared to MM6, related to myeloid categories. **E** GSVA of the marker genes associated with different myeloid cell types. **F** Expression in z-scores of MM dormant cell markers in MM5 and MM6 groups. The MM5 group exhibits enrichment in dormant markers compared to MM6. pDC Plasmacytoid dendritic cells, GMP granulocytes, Granulocyte/macrophage progenitor-granulocytes, GMP Granulocyte/macrophage progenitor, MEP Megakaryocyte/erythroid progenitor, proB B cell progenitor, T NK T Natural killer, CLP Common lymphoid progenitor, HSC Hematopoietic stem cells.

Myeloid TFs regulate the expression of metabolic, myeloid and dormant genes in MM5

To find a connection between metabolic, myeloid and dormant characteristics of group MM5, we analyzed gene regulatory networks using the TraRe (Transcriptional Rewiring) algorithm [22]. This analysis identified myeloid TFs such as NFE2 and CEBPE potentially regulating metabolic, myeloid and dormant genes upregulated in group MM5 (Fig. 3A**;** Supplementary Fig. 3A). The analysis of myeloid TFs expression in groups MM5 and MM6 (in CoMMpass dataset) and also in the two validations cohorts (HOVON-65 and FIMM)), revealed that myeloid TFs were specifically expressed in the group MM5 but were absent in PC from group MM6 (Fig. 3B). Additionally, some myeloid (*ANPEP*, also known as *CD13)* (Fig. 3C), dormant (*BCL2A1* and *GAPT*) (Fig. 3D) and metabolic (*ACSL1* and *ALOX5AP)* (Fig. 3E) genes regulated by myeloid TFs regulons, showed consistent upregulation in group MM5 in comparison to group MM6 (Fig. 3B). These results indicate that myeloid TF regulons are more active and play a regulatory role in the induction of myeloid, dormant and metabolic signatures identify in group MM5. Overexpressed genes identified in MM5 and included in these regulons could have a functional role in MM patients, representing potentially therapeutic targets.

Myeloid genes as biomarkers and therapeutic targets for patients of group MM5

To further investigate the role of myeloid-associated genes in PC from patients in groups MM5 and MM6, we focused on the expression of *CD13* and *CD33*, two myeloid genes that were significantly upregulated in group MM5 (Fig. 3B**;** Supplementary Fig. 4A). The expression of these two genes is associated with poor prognosis in MM patients [35]. In addition, strategies targeting these genes, such as Bestatin for CD13 [36] and CAR-T cell therapies targeting CD33 [37], have been used for the treatment of other human tumors, like acute myeloid leukemia.

First, we investigated the potential impact of *CD13* and *CD33* expression on the prognosis of hyperdiploid MM patients included in groups MM5 (51 patients) and MM6 (171 patients). Patients with high expression of both *CD13* and *CD33* genes (each patient was classified as high *CD13* or/and *CD33* if the expression level for the respective gene exceeded the median expression) had a significantly worse survival compared to patients with low expression (Fig. 4A). Out of the patients with high expression of both genes, 75% belong to group MM5 (Fig. 4A). These results indicate that high expression of *CD13* and *CD33* is a prognostic factor in hyperdiploid patients which on the other hand might represent a therapeutic target in patients with MM and high expression of these genes.

While *CD13* and *CD33* expression in MM5 samples is lower compared to AML patient samples (Supplementary Fig. 4B), we evaluated the antitumor efficacy of Bestatin and the potential of CD33-targeting CAR-T cells against MM cell lines. Treatment of cells from the MM-derived cell line JJN-3 (with CD13 expression) with different concentrations of Bestatin induced a significant reduction in the viability of CD13 + MM cells (Fig. 4B). Similarly, CD33-targeting CAR-Ts showed a significant in vitro antitumoral efficacy in the MM-derived cell line with CD33 expression, RPMI 8226 in comparison with the MM-derived cell line MM.1S, with very low CD33 expression (Fig. 4C**;** Supplementary Fig. 4C, D). These results indicated that myeloid cell characteristics play an important role in the biology of tumor PCs from patients in group MM5 and support the use of therapies directed against MM expressing myeloid markers.

ACSL1 represents a metabolic vulnerability for MM patients

Metabolic vulnerabilities are critical drivers of tumor proliferation across various human cancers, often serving as valuable diagnostic and therapeutic targets [38]. Based on this, we hypothesized that specific metabolic genes dysregulated in the MM5 subgroup might serve as both biomarkers and potential therapeutic targets. Among these, we focused on *ACSL1* (*Acyl-CoA Synthetase Long Chain Family Member 1*), identified as a direct transcriptional target of NFE2 in MM5 patients (Fig. 3). *ACSL1* plays a central role in lipid biosynthesis and fatty acid degradation [39]. Its aberrant expression has been shown to induce metabolic reprogramming in tumor cells, supporting proliferation in multiple solid tumors [40, 41] and, more recently, in MM [42]. Lipid metabolism—particularly pathways involving fatty acid and arachidonic acid metabolism—emerged as the most prominently altered metabolic signature in the MM5 group (Fig. 1D), further underscoring the potential functional relevance of *ACSL1* in this subset.

To explore the clinical significance of *ACSL1* expression, we analyzed its prognostic impact in hyperdiploid MM5 and MM6 patients. Our results revealed that patients from either group with high *ACSL1* expression (each patient was classified as high *ACSL1* if its expression level exceeded the median expression) had significantly worse overall survival compared to those with low expression (Fig. 5A). Strikingly, 100% of MM5 patients exhibited high *ACSL1* expression (Fig. 5A), suggesting a uniform metabolic dependency. These findings support the role of *ACSL1* as a marker of poor prognosis and a potential therapeutic vulnerability in hyperdiploid MM5 patients.

To address the functional role of ACSL1 in MM-PCs, we induced ACSL1 knockdown using two specific CRISPR-Cas9 guides in two MM-derived cell lines. The depletion of ACSL1 (Supplementary Fig. 5A) led to a decrease in viability in MM-PCs (Fig. 5B), suggesting an essential role in MM cells. Transcriptomic analysis following *ACSL1* knockdown revealed a significant downregulation of fatty acyl-CoA biosynthesis and cell cycle-related pathways, as demonstrated by Gene Set Enrichment Analysis (GSEA) in both cell lines (Fig. 5C). Additionally, ACSL1 depletion led to a substantial reduction in mitochondrial respiratory electron transport, consistently observed across both models (Fig. 5C**;** Supplementary Fig. 5B), suggesting a disruption in mitochondrial metabolism.

To validate these findings, we performed Seahorse extracellular flux analysis, which confirmed a significant decrease in both basal and maximal mitochondrial respiratory capacity upon ACSL1 depletion (Fig. 5D). In parallel, ECAR analysis revealed a compensatory increase in glycolytic activity following ACSL1 depletion (Supplementary Fig. 5C), suggesting an active metabolic rewiring from oxidative phosphorylation towards glycolysis rather than a passive consequence of reduced viability. Reduced mitochondrial respiration has been linked to increased sensitivity to the BCL-2 inhibitor Venetoclax [43], implying that *ACSL1* knockdown may sensitize MM cells to anti-apoptotic therapies. Consistent with this hypothesis, dual targeting of *ACSL1*—either via CRISPR-mediated gene disruption or pharmacologic inhibition using Triacsin C (a pan-ACSL inhibitor affecting isoforms 1, 3, 4, and 5)—in combination with Venetoclax or the selective MCL1 inhibitor S63845, produced a robust and statistically significant synergistic reduction in MM-PC viability (Fig. 5E–G).

To further validate the translational relevance of these findings, we evaluated the role of ACSL1 in MM progression and the therapeutic impact of its inhibition in combination with anti-apoptotic agents in vivo using a subcutaneous MM xenograft model. MM.1S cells either expressing ACSL1 or lacking ACSL1 expression (scramble and sgACSL1-1 groups, respectively; $n = 6$ per group) were injected into BALB/cA $Rag2^{-/-}\gamma c^{-/-}$ mice. In parallel, mice were treated with Venetoclax or the selective MCL1 inhibitor S63845 either as single agents or in combination with ACSL1 depletion. Consistent with our in vitro observations, ACSL1 depletion significantly impaired tumor growth compared to control tumors (Fig. 5H). Importantly, the combination of ACSL1 depletion with either Venetoclax (Fig. 5H, upper panel) or S63845 (Fig. 5H, lower panel) produced a markedly stronger antitumoral effect than either single-agent treatment or ACSL1 depletion alone, resulting in reduced tumor burden and delayed tumor progression. These findings further support the notion that ACSL1

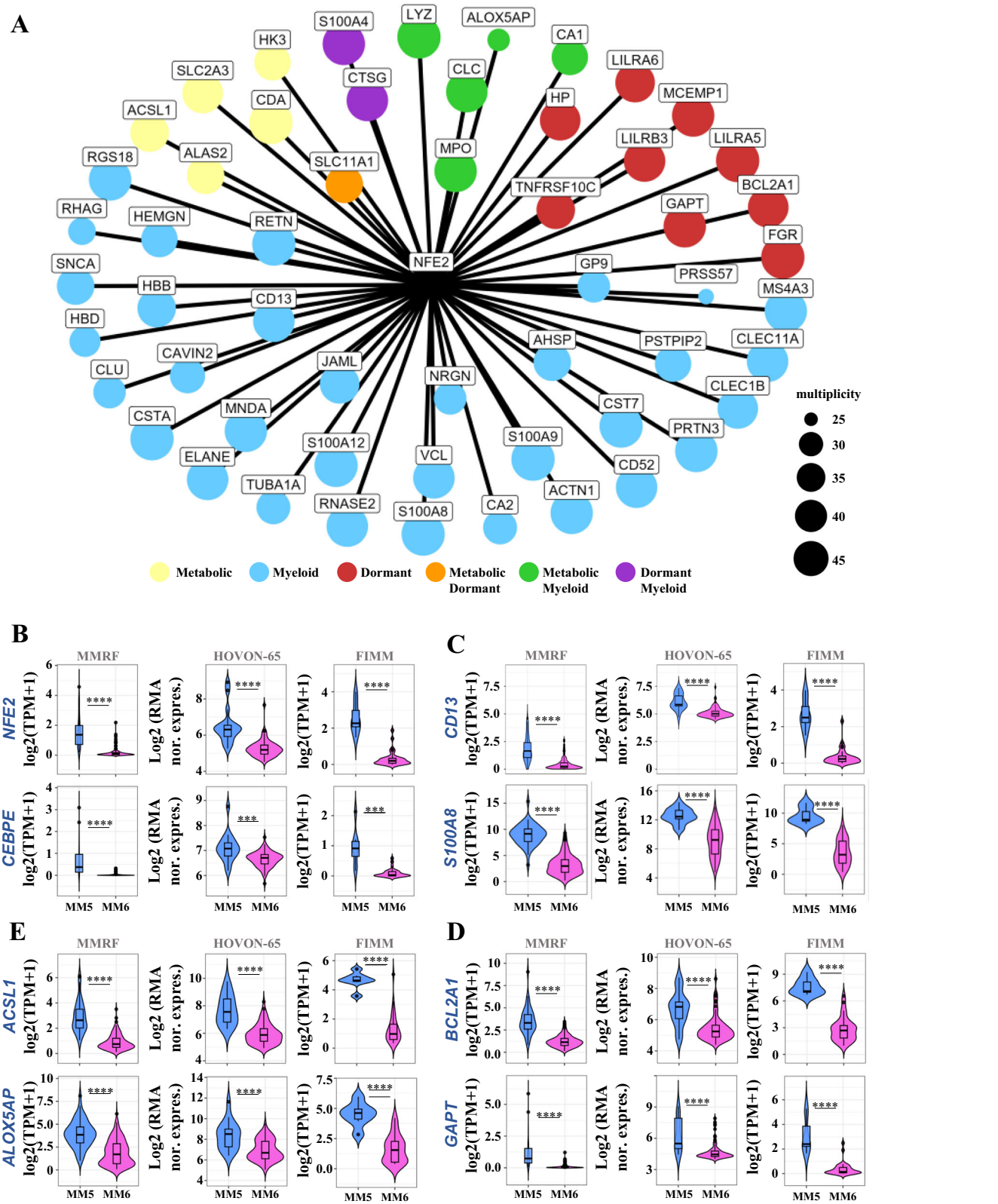

Fig. 3 Myeloid TF regulates the dormant and metabolic characteristics of MM patients of MM5 group. A TraRE analysis showing that the myeloid transcription factor NFE2 regulates metabolic, myeloid, and dormant genes upregulated in MM5. Boxplots displaying the expression levels of myeloid TFs (**B**), myeloid markers (**C**), dormant markers (**D**), and metabolic signature genes (**E**) in MM5 and MM6 patients from the MMRF, HOVON-65, and FIMM MM cohorts.

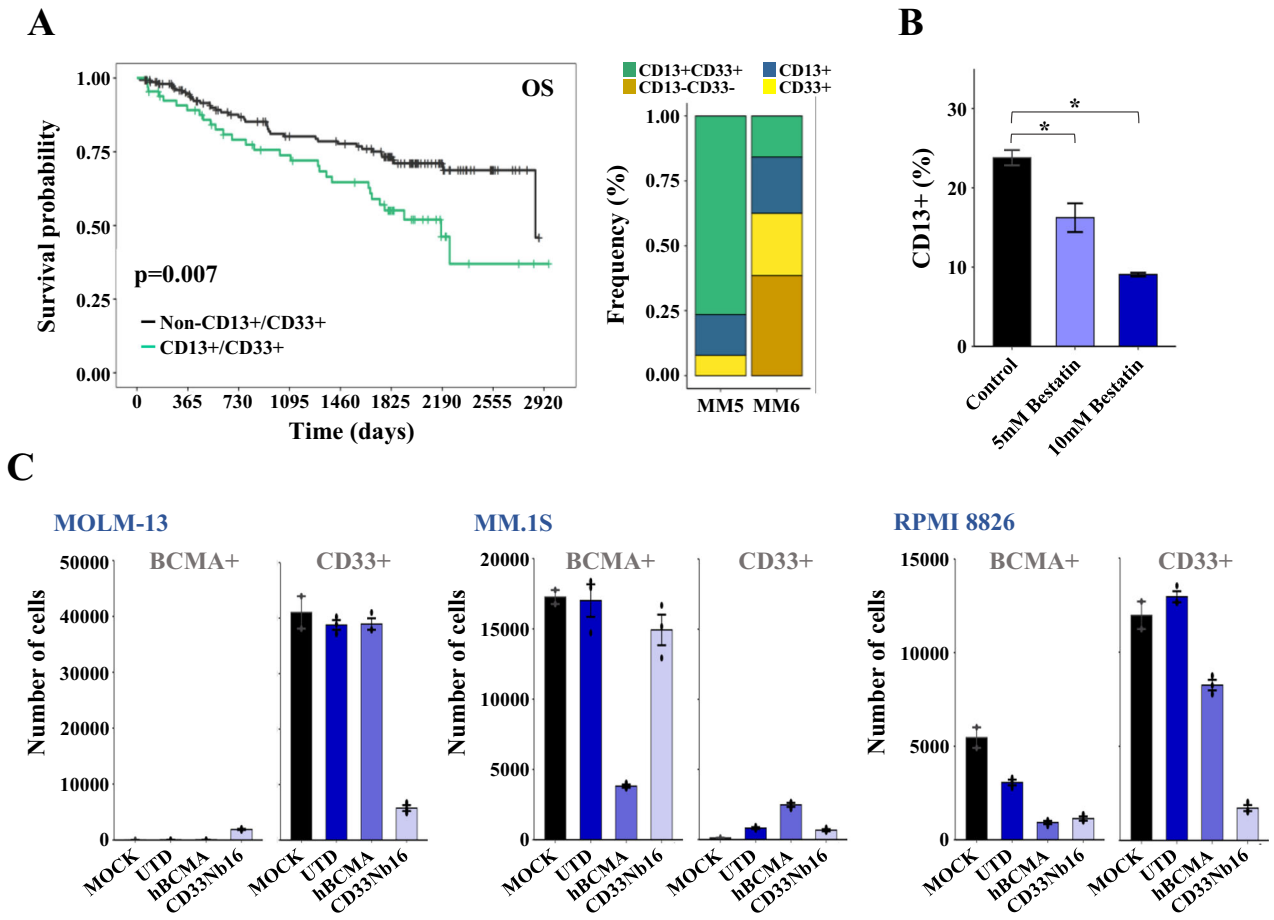

Fig. 4 Myeloid genes *CD13* and *CD33* as biomarkers and therapeutic targets in MM5 patients. A Overall Survival (OS) analysis of MM5 and MM6 patients stratified by *CD13* and *CD33* gene expression. The green curve represents MM5 and MM6 patients with high expression of both *CD13* and *CD33*, while the black curve corresponds to the remaining MM5 and MM6 patients. Bar plots show the percentage of patients with high expression of each gene. **B** Percentage of CD13+ cells in JJN-3 cell cultures before and after Bestatin treatment. Data are presented as mean values +/− S.D. of three biological replicates. Statistical significance was calculated using the Mann-Whitney U test. *$p \leq 0.05$. **C** Proportion of BCMA$^+$ (left panels) and CD33$^+$ (right panels) cells in MOLM-13 (AML), MM.1S and RPMI-8226 (MM) cell lines following co-culture with different T-cell conditions. For each cell line and antigen, four conditions are shown: Mock, untransduced T cells (UTD), BCMA-targeting CAR-T cells (hBCMA), and CD33-targeting CAR-T cells (CD33Nb16). BCMA CAR-T cells were used as a positive control in MM cell lines. Data are presented as mean ± S.D. of three technical replicates.

inhibition sensitizes MM cells to BCL2- and MCL1-targeted therapies in vivo.

Together, these results indicate that *ACSL1* is a critical metabolic dependency in MM5 cells. Its depletion perturbs mitochondrial function and enhances the efficacy of anti-apoptotic agents, offering a promising therapeutic strategy for targeting high-risk MM5 patients.

The expression of S100A8 gene identifies patients from group MM5

Given the potential for a therapeutic strategy targeting MM5 hyperdiploid patients, we aimed to identify a biomarker for patients in groups MM5 and MM6. We selected all patients from the CoMMpass cohort classified into MM5 and MM6 hyperdiploid groups and randomly split the cohort into an 80% training set and 20% test set, maintaining the proportional representation of the two hyperdiploid groups. First, we performed a differential gene expression analysis between MM5 and MM6 patients in the training set, detecting 933 upregulated genes (logFC > 2, *adjusted p-value* < 0.05 and *B value* > 10) in MM5 patients. Subsequently, in order to obtain the most robust and easy-to-analyze biomarker among the differentially expressed genes, we further refined our selection by focusing on genes with a median expression difference of at least 300 TPMs between the two groups. This analysis revealed the expression of *S100A8*, *S100A9*, and *HBB* genes as candidate biomarkers. To construct an effective predictive model, we calculated the pairwise correlations between the expression levels of the three candidate genes and excluded *S100A9* and HBB due to their high correlation (>0.9) with *S100A8*. Finally, we developed a linear model using a binomial family for classification (Fig. 6A). In the test set, we observed that the expression of the *S100A8* gene successfully identified MM5 hyperdiploid patients with an accuracy higher than 0.9 (Fig. 6B-C). This result was confirmed in an additional cohort of MM patients (FIMM cohort). In conclusion, the analysis of the expression of a single gene allows the identification of MM5 patients among MM5 and MM6 hyperdiploid MM patients.

DISCUSSION

The inter-tumoral biological heterogeneity of MM remains a major contributor to its clinical intractability [1, 2, 11, 44, 45]. In this study, we introduce a novel and clinically actionable stratification of MM based on metabolic transcriptome profiling, identifying six distinct subgroups with specific metabolic signatures. Remarkably,

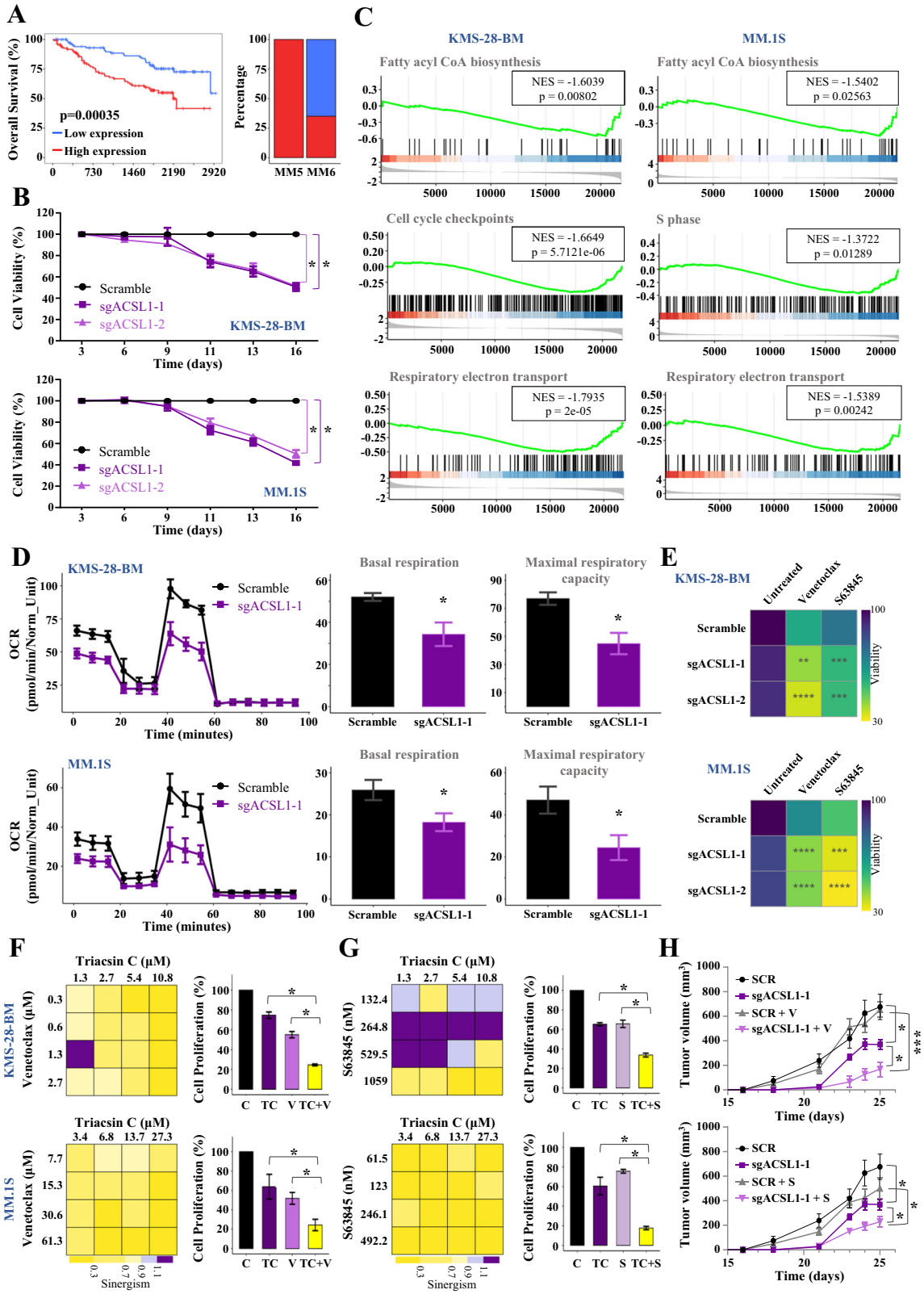

these subgroups exhibit distinct metabolic programs and, while they do not correlate with conventional risk stratifications used in MM, they are strongly associated with canonical cytogenetic abnormalities characteristic of the disease. Consistent with this robust correlation, the impact of these metabolic transcriptome groups on the overall survival of MM patients was associated with specific cytogenetic alterations. However, a striking exception emerged within hyperdiploid MM, which is traditionally considered to confer a favorable prognosis: patients in the MM5 subgroup exhibited a significantly poorer outcome

Fig. 5 The metabolic gene *ACSL1* is an essential and therapeutic target in hyperdiploid MM5 patients. A Overall Survival (OS) analysis of MM5 and MM6 patients based on *ACSL1* expression levels, along with a bar plot showing the percentage of patients in each group with high or low *ACSL1* expression. **B** Cell viability of ACSL1-deficient KMS-28-BM and MM.1S cell lines obtained by CRISPR-Cas9 technology with two different sgRNAs. The viability percentage is normalized to cells infected with an empty vector (Scramble, black line). This experiment was performed in three different biological replicates. Data are presented as mean values +/- S.D. **C** GSEA analysis of altered pathways from RNA-seq data of ACSL1-deficient KMS-28-BM and MM.1S cell lines. **D** Seahorse assay measuring oxygen consumption rate (OCR) as an indicator of mitochondrial respiration. Data are presented as mean values +/− S.D. of three biological replicates. Statistical significance was calculated using the Mann-Whitney U test. *$p \leq 0.05$. **E** Synergy experiments testing ACSL1 knockdown (via two distinct CRISPR guides) in combination with Venetoclax or S63845 (a selective MCL1 inhibitor) in KMS-28-BM and MM.1S MM cell lines. P values were determined by one-way analysis of variance (ANOVA), followed by Tukey's multiple comparison test. Data represent the mean of three biological replicates. *$p \leq 0.05$; **$p \leq 0.01$; ***$p \leq 0.001$; ****, $p \leq 0.0001$. **F** Synergy experiments combining ACSL1 inhibition using Triacsin C (TriC - an inhibitor of ACSL1, 3, 4, and 5) with Venetoclax in KMS-28-BM and MM.1S MM cell lines. The heatmap represents the combination index (CI), categorized as follows: <0.3 (strong synergism), 0.3–0.7 (synergism), 0.7-0.9 (moderate synergism), 0.9-1.1 (nearly additive), and >1.1 (antagonism). Specifically, the data shown represent the mean of three biologically independent experiments. In the bar plot, cell proliferation for a specific combination is depicted as mean values +/- S.D. from three biological replicates. Statistical significance was calculated using the Mann-Whitney U test. *$p \leq 0.05$. C Untreated control cells, TC Triacsin C; V Venetoclax; TC + V combination of Triacsin C and Venetoclax. **G** Synergy experiments combining ACSL1 inhibition using Triacsin C with S63845 (MCL1 inhibitor) in KMS-28-BM and MM.1S MM cell lines. The heatmap represents the combination index (CI), categorized as follows: <0.3 (strong synergism), 0.3–0.7 (synergism), 0.7-0.9 (moderate synergism), 0.9-1.1 (nearly additive), and >1.1 (antagonism). Specifically, the data shown represent the mean of three biologically independent experiments. In the bar plot, cell proliferation for a specific combination is depicted as mean values +/− S.D. from three biological replicates. Statistical significance was calculated using the Mann-Whitney U test. *$p \leq 0.05$. C Untreated control cells, TC Triacsin C, S = S63845, TC + S = combination of Triacsin C and S63845. **H** In vivo evaluation of ACSL1 depletion in combination with anti-apoptotic therapies in a subcutaneous MM xenograft model. Tumor growth curves of BALB/cA Rag2$^{-/-}$γc$^{-/-}$ mice ($n = 6$ mice per group) injected with MM.1S scramble or sgACSL1-1 cells and treated with Venetoclax (upper panel) or S63845 (lower panel). Tumor volume was monitored longitudinally by caliper measurements. Data are represented as mean ± SEM. Statistical significance was calculated using a parametric t-test. SCR Scramble, V Venetoclax, S S63845.

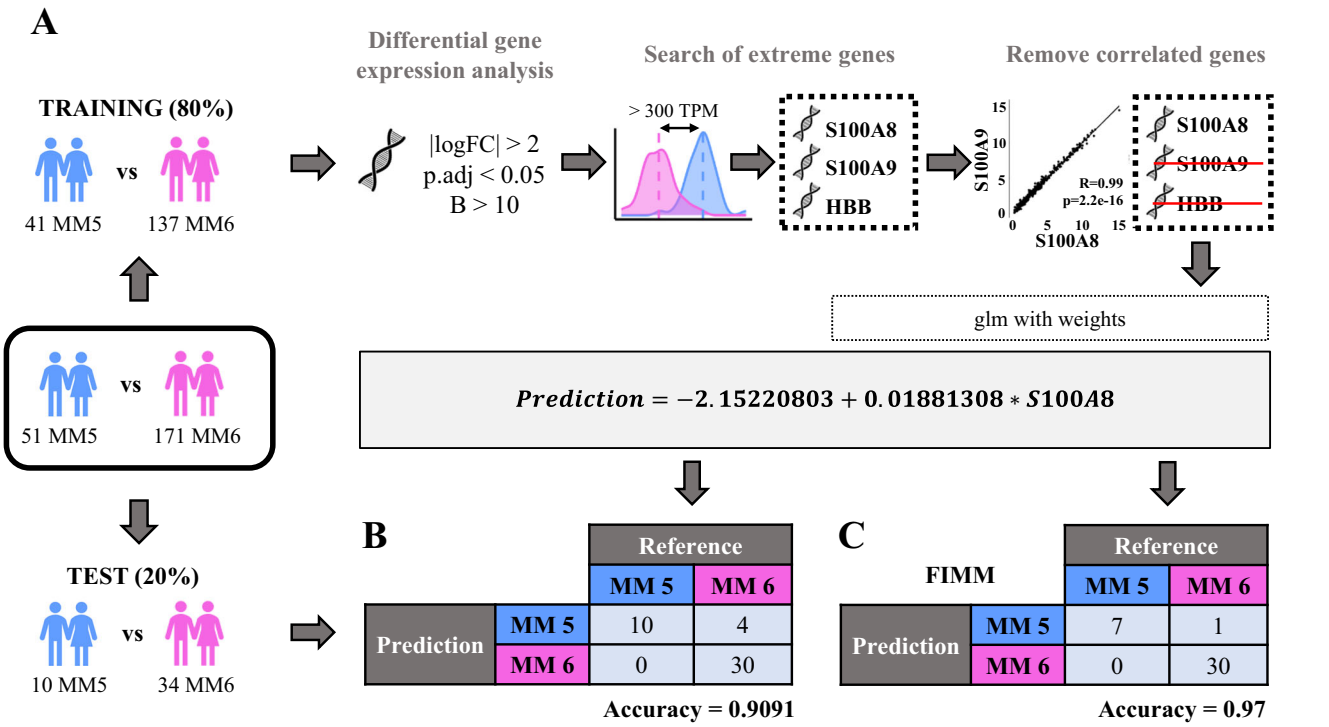

Fig. 6 *S100A8* gene is a biomarker for differentiating the hyperdiploid groups. A Graphical representation of the biomarker selection process for MM5 patients within the MM5 and MM6 hyperdiploid subgroup.

compared to those in MM6, despite sharing similar cytogenetic features [3]. This finding highlights the added resolution provided by metabolic transcriptomic classification and its potential to refine risk stratification even within genetically homogeneous subgroups. Furthermore, the identification of distinct metabolic signatures within these cytogenetic subgroups suggests the presence of subgroup-specific metabolic vulnerabilities that could be therapeutically exploited.

Among the six identified metabolic transcriptome groups, we specifically focused on understanding the factors contributing to the poorer overall survival observed in hyperdiploid MM5 patients. Unexpectedly, tumor PCs from MM5 patients showed significantly increased expression and enrichment of pathways associated with myeloid progenitor cells, despite MM being a lymphoid neoplasm. Our findings are consistent with those of Khoo et al., who demonstrated that dormant MM cells localize to specific bone marrow niches and display a transcriptome enriched in myeloid differentiation genes [34]. In line with their study, we show that MM5 plasma cells express markers of dormancy and myeloid lineage, suggesting that a dormant-like state -regulated by

myeloid transcription factors- may underlie therapy resistance and poor prognosis in MM5 patients.

Our regulatory network analysis further supports this model, identifying myeloid TFs such as NFE2 as key drivers of the metabolic, myeloid, and dormancy-related transcriptional programs observed in MM5. These results suggest that tumor–niche interactions, particularly within the endosteal niche, may induce transcriptional rewiring that confers a survival advantage to MM5 cells under therapeutic pressure as described by Khoo et al. [34]. The endosteal niche is the primary bone marrow microenvironment supporting the dormant functions of MM cells, and it is directly implicated in MM oncogenesis and clinical outcomes [46, 47]. Further spatial and functional studies exploring the interaction between MM5 plasma cells and their microenvironment will be critical for understanding the biology of dormancy and its clinical implications.

Building on these insights, we identified therapeutic vulnerabilities associated with the MM5 phenotype. The myeloid antigens CD13 and CD33—upregulated in MM5—are traditionally targeted in myeloid malignancies [36, 37]. We demonstrate that the inhibition of CD13 with Bestatin and targeting of CD33 with CAR-T cells both reduce MM cell viability in vitro, supporting the rationale for repurposing myeloid-targeted therapies in this MM subgroup.

In addition, we identified *ACSL1* as an essential metabolic gene in MM5 cells. ACSL1 is a member of the acyl-coenzyme A long-chain synthetase (ACSL) family of proteins, which have been involved in the proliferation of various human tumors [39–41]. Inhibition of the ACSL family of proteins has shown significant anti-tumoral effects in solid tumors such as lung [48], breast [49], or prostate [41] cancers, as well as in hematological neoplasms like acute myeloid leukemia [50]. Recently, Murphy et al. reported the efficacy of ACSL inhibition in MM [42]. Our findings not only confirm its role in MM but also reveal an unrecognized mechanism in MM previously observed in prostate cancer [41]: ACSL1 knockdown significantly reduced the respiratory electron transport in mitochondria [43], and as a consequence sensitizes myeloma cells to anti-apoptotic inhibitors, such as Venetoclax. Venetoclax-based regimens have been used for MM patients, particularly for patients harboring the t(11:14) translocation [43, 51]. However, resistance [52] to Venetoclax remains a significant challenge, highlighting the need for the development of novel therapeutic strategies to overcome it. Interestingly, in our study, we demonstrated that ACSL1 is an important metabolic vulnerability whose depletion enhances the sensitivity of MM cells to Venetoclax and other antiapoptotic inhibitors, offering, with this combination, an effective therapeutic strategy for this particular group of MM patients.

Finally, we sought to translate our findings into a clinically useful biomarker. We identified *S100A8* as a highly expressed gene capable of discriminating MM5 from MM6 hyperdiploid patients with high accuracy. This simple biomarker has the potential to facilitate patient stratification and guide personalized therapeutic interventions in clinical practice.

In summary, our study provides a comprehensive metabolic classification of MM and identifies a clinically relevant MM5 subgroup characterized by myeloid and dormant features, metabolic dependency on *ACSL1*, and poor prognosis. These findings offer novel biomarkers and therapeutic opportunities and highlight the importance of integrating metabolic profiling into the clinical framework of MM to enable precision medicine approaches.

DATA AVAILABILITY

RNA-seq data generated in this study have been deposited in NCBI Gene Expression Omnibus (GEO) repository under the accession number GSE297305.

REFERENCES

1. Mateos MV, Cavo M, Blade J, Dimopoulos MA, Suzuki K, Jakubowiak A, et al. Overall survival with daratumumab, bortezomib, melphalan, and prednisone in newly diagnosed multiple myeloma (ALCYONE): a randomised, open-label, phase 3 trial. Lancet. 2020;395:132–41.
2. Cardona-benavides IJ, de Ramón C, Gutiérrez NC. Genetic abnormalities in multiple myeloma: Prognostic and therapeutic implications. Cells. 2021;10:1–28.
3. Braggio E, Kortüm KM, Stewart AK. SnapShot: multiple myeloma. Cancer Cell. 2015;28:678–678.e1.
4. Hanahan D. Hallmarks of cancer: new dimensions. Cancer Discov. 2022;12:31–46.
5. Li L, Wei Y, To C, Zhu CQ, Tong J, Pham NA, et al. Integrated Omic analysis of lung cancer reveals metabolism proteome signatures with prognostic impact. Nat Commun. 2014;5:1–12.
6. Korangath P, Teo WW, Sadik H, Han L, Mori N, Huijts CM, et al. Targeting glutamine metabolism in breast cancer with aminooxyacetate. Clin Cancer Res. 2015;21:3263–73.
7. Cutruzzolà F, Giardina G, Marani M, Macone A, Paiardini A, Rinaldo S, et al. Glucose metabolism in the progression of prostate cancer. Front Physiol. 2017;8:246811.
8. Liu M, Wang Y, Miettinen JJ, Kumari R, Majumder MM, Tierney C, et al. S100 calcium binding protein family members associate with poor patient outcome and response to proteasome inhibition in multiple myeloma. Front Cell Dev Biol. 2021;9:2261.
9. Thongon N, Ma F, Baran N, Lockyer P, Liu J, Jackson C, et al. Targeting DNA2 overcomes metabolic reprogramming in multiple myeloma. Nat Commun. 2024;15:1–13.
10. Agirre X, Meydan C, Jiang Y, Garate L, Doane AS, Li Z, et al. Long non-coding RNAs discriminate the stages and gene regulatory states of human humoral immune response. *Nat Commun* 2019; 10. https://doi.org/10.1038/s41467-019-08679-z.
11. Carrasco-Leon A, Ezponda T, Meydan C, Valcárcel LV, Ordoñez R, Kulis M, et al. Characterization of complete lncRNAs transcriptome reveals the functional and clinical impact of lncRNAs in multiple myeloma. Leukemia. 2021;35:1438–50.
12. Broyl A, Hose D, Lokhorst H, De Knegt Y, Peeters J, Jauch A, et al. Gene expression profiling for molecular classification of multiple myeloma in newly diagnosed patients. Blood. 2010;116:2543–53.
13. Bengtsson H, Simpson K, Bullard J, Hansen K aroma.affymetrix: A generic framework in R for analyzing small to very large Affymetrix data sets in bounded memory. *Methods* 2008; Tech Repor: 1–9.
14. Possemato R, Marks KM, Shaul YD, Pacold ME, Kim D, Birsoy K et al. Functional genomics reveal that the serine synthesis pathway is essential in breast cancer. 2011. https://doi.org/10.1038/nature10350.
15. Wang J, Wen S, Fraser Symmans W, Pusztai L, Coombes KR. The bimodality index: A criterion for discovering and ranking bimodal signatures from cancer gene expression profiling data. Cancer Inf. 2009;7:199–216.
16. Gaujoux R, Seoighe C. A flexible R package for nonnegative matrix factorization. BMC Bioinforma. 2010;11:1–9.
17. Liberzon A, Subramanian A, Pinchback R, Thorvaldsdóttir H, Tamayo P, Mesirov JP. Molecular signatures database (MSigDB) 3.0. Bioinformatics. 2011;27:1739–40.
18. Subramanian A, Tamayo P, Mootha VK, Mukherjee S, Ebert BL, Gillette MA, et al. Gene set enrichment analysis: A knowledge-based approach for interpreting genome-wide expression profiles. Proc Natl Acad Sci USA. 2005;102:15545–50.
19. Hänzelmann S, Castelo R, Guinney J. GSVA: Gene set variation analysis for microarray and RNA-Seq data. BMC Bioinforma. 2013;14:1–15.
20. Ainciburu M, Ezponda T, Berastegui N, Alfonso-Pierola A, Vilas-Zornoza A, Martin-Uriz PS et al. Uncovering perturbations in human hematopoiesis associated with healthy aging and myeloid malignancies at single-cell resolution. *Elife* 2023; 12. https://doi.org/10.7554/eLife.79363.
21. Wu J, Xiao Y, Sun J, Sun H, Chen H, Zhu Y, et al. A single-cell survey of cellular hierarchy in acute myeloid leukemia. J Hematol Oncol. 2020;13:1–19.
22. De La Fuente Cedeño J, Hernaez M, Blatti C TraRe: Transcriptional Rewiring. 2022.https://github.com/ubioinformat/TraRe/tree/master.
23. Lambert SA, Jolma A, Campitelli LF, Das PK, Yin Y, Albu M, et al. The Human Transcription Factors. Cell. 2018;172:650–65.
24. Rodriguez-Marquez P, Calleja-Cervantes ME, Serrano G, Oliver-Caldes A, Palacios-Berraquero ML, Martin-Mallo A, et al. CAR density influences antitumoral efficacy of BCMA CAR T cells and correlates with clinical outcome. Sci Adv. 2022;8:514.
25. Bernasconi-Bisio F, Molina E, Ibarra V, Ibáñez-Sala I, Rochira F, Jauregui P, et al. Discovery and preclinical development of a SdAb-based CAR-T technology for targeting CD33 in AML. Mol Ther Oncol. 2025;33:200949.
26. Ordoñez R, Kulis M, Russiñol N, Chapaprieta V, Carrasco-Leon A, García-Torre B, et al. Chromatin activation as a unifying principle underlying pathogenic mechanisms in multiple myeloma. Genome Res. 2020;30:1217–27.

27. Zhang Y, Parmigiani G, Johnson WE. ComBat-seq: Batch effect adjustment for RNA-seq count data. *NAR Genomics Bioinforma* 2020; 2. https://doi.org/10.1093/nargab/lqaa078.
28. Palumbo A, Avet-Loiseau H, Oliva S, Lokhorst HM, Goldschmidt H, Rosinol L, et al. Revised international staging system for multiple myeloma: A report from the International Myeloma Working Group. J Clin Oncol. 2015;33:2863–9.
29. Avet-Loiseau H, Davies FE, Samur MK, Corre J, D'agostino M, Kaiser MF et al. International Myeloma Society/International Myeloma Working Group Consensus Recommendations on the Definition of High-Risk Multiple Myeloma. J Clin Oncol 2025. https://doi.org/10.1200/JCO-24-01893/SUPPL_FILE/DS_JCO-24-01893.PDF.
30. Bailur JK, McCachren SS, Doxie DB, Shrestha M, Pendleton K, Nooka AK et al. Early alterations in stem-like/marrow-resident T cells and innate and myeloid cells in preneoplastic gammopathy. JCI Insight 2019; **4**. https://doi.org/10.1172/jci.insight.127807.
31. Johnson TS, Sudha P, Liu E, Becker N, Robertson S, Blaney P, et al. 1q amplification and PHF19 expressing high-risk cells are associated with relapsed/refractory multiple myeloma. Nat Commun. 2024;15:4144.
32. Liu R, Gao Q, Foltz SM, Fowles JS, Yao L, Wang JT, et al. Co-evolution of tumor and immune cells during progression of multiple myeloma. Nat Commun. 2021;12:2559.
33. Maura F, Boyle EM, Coffey D, Maclachlan K, Gagler D, Diamond B, et al. Genomic and immune signatures predict clinical outcome in newly diagnosed multiple myeloma treated with immunotherapy regimens. Nat Cancer. 2023;4:1660–74.
34. Khoo WH, Ledergor G, Weiner A, Roden DL, Terry RL, McDonald MM, et al. A niche-dependent myeloid transcriptome signature defines dormant myeloma cells. Blood. 2019;134:30–43.
35. Shim H, Ha JH, Lee H, Sohn JY, Kim HJ, Eom HS, et al. Expression of Myeloid Antigen in Neoplastic Plasma Cells Is Related to Adverse Prognosis in Patients with Multiple Myeloma. Biomed Res Int 2014; 2014. https://doi.org/10.1155/2014/893243.
36. Mishima Y, Matsumoto-Mishima Y, Terui Y, Katsuyama M, Yamada M, Mori M, et al. Leukemic cell-surface CD13/aminopeptidase N and resistance to apoptosis mediated by endothelial cells. J Natl Cancer Inst. 2002;94:1020–8.
37. Calviño C, Ceballos C, Alfonso A, Jauregui P, Calleja-Cervantes ME, San Martin-Uriz P, et al. Optimization of universal allogeneic CAR-T cells combining CRISPR and transposon-based technologies for treatment of acute myeloid leukemia. Front Immunol. 2023;14:1270843.
38. Altea-Manzano P, Decker-Farrell A, Janowitz T, Erez A. Metabolic interplays between the tumour and the host shape the tumour macroenvironment. Nat Rev Cancer 2025; 1–19.
39. Paul DS, Grevengoed TJ, Pascual F, Ellis JM, Willis MS, Coleman RA. Deficiency of cardiac Acyl-CoA synthetase-1 induces diastolic dysfunction, but pathologic hypertrophy is reversed by rapamycin. Biochim Biophys Acta - Mol Cell Biol Lipids. 2014;1841:880–7.
40. Fu H, Han X, Guo W, Zhao X, Yu C, Zhao W, et al. Cystathionine-γ-lyase contributes to tamoxifen resistance, and the compound I194496 alleviates this effect by inhibiting the PPARγ/ACSL1/STAT3 signalling pathway in oestrogen receptor-positive breast cancer. Sci Rep. 2024;14:22988.
41. Ma Y, Zha J, Yang XK, Li Q, Zhang Q, Yin A, et al. Long-chain fatty acyl-CoA synthetase 1 promotes prostate cancer progression by elevation of lipogenesis and fatty acid beta-oxidation. Oncogene. 2021;40:1806–20.
42. Murphy CS, Fairfield H, DeMambro VE, Fadel S, Gartner CA, Karam M, et al. Inhibition of acyl-CoA synthetase long-chain isozymes decreases multiple myeloma cell proliferation and causes mitochondrial dysfunction. Mol Oncol 2025. https://doi.org/10.1002/1878-0261.13794.
43. Bajpai R, Sharma A, Achreja A, Edgar CL, Wei C, Siddiqa AA, et al. Electron transport chain activity is a predictor and target for venetoclax sensitivity in multiple myeloma. Nat Commun. 2020;11:1–16.
44. Agirre X, Castellano G, Pascual M, Heath S, Kulis M, Segura V, et al. Whole-epigenome analysis in multiple myeloma reveals DNA hypermethylation of B cell-specific enhancers. Genome Res. 2015;25:478–87.
45. Maura F, Rajanna AR, Ziccheddu B, Poos AM, Derkach A, MacLachlan K, et al. Genomic classification and individualized prognosis in multiple myeloma. J Clin Oncol. 2024;42:1229–40.
46. Capp JP, Bataille R. The ins and outs of endosteal niche disruption in the bone marrow: relevance for myeloma oncogenesis. Biology. 2023;12:990.
47. Morris EV, Edwards CM. Morphogens and growth factor signalling in the myeloma bone-lining niche. Cell Mol Life Sci. 2021;78:4085–93.
48. Ma Y, Nenkov M, Berndt A, Abubrig M, Schmidt M, Sandhaus T, et al. The diagnostic value of ACSL1, ACSL4, and ACSL5 and the clinical potential of an ACSL inhibitor in non-small-cell lung cancer. Cancers. 2024;16:1170.
49. Ahmad R, Thomas R, Al-Rashed F, Akhter N, Al-Mulla F. Acsl1 regulates tnfα-induced gm-csf production by breast cancer mda-mb-231 cells. Biomolecules. 2019;9:555.
50. Ye W, Wang J, Huang J, He X, Ma Z, Li X, et al. ACSL5, a prognostic factor in acute myeloid leukemia, modulates the activity of Wnt/β-catenin signaling by palmitoylation modification. Front Med. 2023;17:685–98.
51. Deng S, Derebail S, Weiler VJ, Ng JF, Maroto-Martin E, Chatterjee M, et al. Venetoclax resistance leads to broad resistance to standard-of-care anti-MM agents, but not to immunotherapies. Blood Adv. 2024;8:4025–34.
52. Nair R, Vu AH, Freer AK, Bhatia KS, Wang D, Savani MR, et al. Heme promotes venetoclax resistance in multiple myeloma through MEK-ERK signaling and purine biosynthesis. Blood. 2025;145:732–747.

ACKNOWLEDGEMENTS

We thank the Biobank of the University of Navarra for its collaboration. This research was funded by grants from the Instituto de Salud Carlos III (ISCIII) and co-financed by the European Union: PI20/01308, PI22/00947, PI23/00488, PI23/00516, PI25/01281, PMP21/00015 (PREGENLINF) and CIBERONC CB16/12/00489 and Miguel Servet contract (CP22/00005). Gobierno de Navarra: Department of Health (GNS_44-2021; GN2023/11) (also co-financed by FEDER) and Department of Economic Development 0011-1411-2022-000068, 0011-1411-2022-000077 (NANO-RC), 0011-1411-2023-000074, 0011-1411-2023-000105 (DIAMANTE) and NANO-Protacs and with support from 616/C/2019 Fundació La Marató de TV3. The study was also supported by Paula and Rodger Riney Foundation.

AUTHOR CONTRIBUTIONS

Conception and design: NB, ESJ-E, FJ-P, FP and XA. Development of methodology: NB, ESJ-E, LV-V, DO-M, FJ-P, FP and XA. Acquisition of data and assistance with experiments: NB, ESJ-E, LV-V, DO-M, EU-C, LG, EM, PR-M, RK, PSM-U, JRR-M, LP-C, CA-H, PR-O and XA. Analysis and interpretation of data: NB, ESJ-E, LV-V, DO-M, FJ-P, FP and XA. Writing, review, and/or revision of the manuscript: NB, ESJ-E, LV-V, DO-M, FJ-P, FP and XA. Study supervision: FJ-P, FP and XA.

FUNDING

F.P. discloses support for the research of this work from the Instituto de Salud Carlos III (ISCIII) and co-financed by the European Union: PI20/01308, PI23/00516, PMP21/00015 (PREGENLINF) and CIBERONC CB16/12/00489. Gobierno de Navarra: Department of Economic Development 0011-1411-2022-000068, 0011-1411-2022-000077 (NANO-RC), 0011-1411-2023-000074, 0011-1411-2023-000105 (DIAMANTE) and NANO-Protacs. The study was also supported by the Paula and Rodger Riney Foundation. E. SJ-E. discloses support for the research of this work from the Instituto de Salud Carlos III (ISCIII) and co-financed by the European Union: PI23/00488. Gobierno de Navarra: Department of Health (GN2023/11) (also co-financed by FEDER). X. A. discloses support for the research of this work from the Instituto de Salud Carlos III (ISCIII) and co-financed by the European Union: PI22/00947, PI25/01281. Gobierno de Navarra: Department of Health (GNS_44-2021) (also co-financed by FEDER) and Department of Economic Development 0011-1411-2022-000077 (NANO-RC) and NANO-Protacs and with support from 616/C/2019 Fundació La Marató de TV3. L.P-C. discloses support for the research of this work from the Instituto de Salud Carlos III (ISCIII) and co-financed by FEDER: Miguel Servet contract (CP22/00005). The rest of the authors declare no relevant funding.

COMPETING INTERESTS

The authors declare no competing interests.

ADDITIONAL INFORMATION

Supplementary information The online version contains supplementary material available at https://doi.org/10.1038/s41408-026-01604-w.

Correspondence and requests for materials should be addressed to Francisco J. Planes , Xabier Agirre or Felipe Prósper.

Reprints and permission information is available at http://www.nature.com/reprints

Publisher's note Springer Nature remains neutral with regard to jurisdictional claims in published maps and institutional affiliations.

Open Access This article is licensed under a Creative Commons Attribution-NonCommercial-NoDerivatives 4.0 International License, which permits any non-commercial use, sharing, distribution and reproduction in any medium or format, as long as you give appropriate credit to the original author(s) and the source, provide a link to the Creative Commons licence, and indicate if you modified the licensed material. You do not have permission under this licence to share adapted material derived from this article or parts of it. The images or other third party material in this article are included in the article's Creative Commons licence, unless indicated otherwise in a credit line to the material. If material is not included in the article's Creative Commons licence and your intended use is not permitted by statutory regulation or exceeds the permitted use, you will need to obtain permission directly from the copyright holder. To view a copy of this licence, visit http://creativecommons.org/licenses/by-nc-nd/4.0/.

© The Author(s) 2026